

Droplet formation in first order phase transitions with long range Coulomb interaction.

J. Lorenzana*, C. Castellani, and C. Di Castro

Dipartimento di Fisica, Università di Roma "La Sapienza" and Istituto Nazionale di Fisica della Materia, Unità di Roma I, Piazzale A. Moro 2, I-00185 Roma, Italy.

(December 2, 2024)

We analyze the combined effect of the long range Coulomb (LRC) interaction and of surface energy on first order density-driven phase transitions between two phases in the presence of a compensating rigid background. In the coexistence region we study a mixed state formed of bubbles of one phase into the other in the case in which the scale of the inhomogeneities is much larger than the interparticle distance. We derive the general equations for the chemical potential and the pressures of each phase and generalize the Maxwell construction to this situation. We find that quite generally the transition to the mixed state is abrupt i.e. drops of the first phase appear with a finite value of the radius and of the phase volume fraction. Contrary to the ordinary Maxwell construction, the inverse specific volume of each phase depends here on the global density in the coexistence region and can decrease as the global density increases. The range of densities in which coexistence is observed shrinks as the LRC interaction increases until it reduces to a singular point. We argue that close to this singular point the system undergoes a lattice instability as long as the inverse lattice compressibility is finite. These general ideas are applied to the low density electron gas and to electronic phase separation in the low density three dimensional $t - J$ model and in the manganites near the charge ordered phase. For the low density electron gas we find that the well known apparent instabilities at low densities do not lead to macroscopic drop formation. For the $t - J$ model we find that the LRC interaction significantly modifies the phase diagram favoring uniform phases and mixed states of antiferromagnetic (AF) regions surrounded by metallic regions over AF regions surrounded by empty space. For the manganites we show that the dependence of local densities of the phases on the overall density gives a non-monotonous behavior of the Curie temperature on doping in agreement with experiments.

Pacs Numbers: 64.75.1g 71.10.Hf 71.10.Ca 75.30.Vn

I. INTRODUCTION

The complex phase-diagrams of hole doped cuprates and manganites have rekindled the study of mixed states in modeling these systems.^{1–3} Indeed strongly correlated systems with narrow bandwidth and short range interactions show a generic tendency to phase separate into hole-rich and hole-poor regions. When long range Coulomb (LRC) forces are taken into account this instability with macroscopic separation is frustrated due to the electrostatic energy cost and this can lead to charge inhomogeneous states of various nature,^{4–7} where domains of various forms of one phase (B) are embedded in the other phase (A).

In the inhomogeneous state the charge is segregated locally over some characteristic distance but the overall density (averaged over much larger distances) is a fixed constant in order to guarantee large scale neutrality and avoid the large Coulomb cost. Such a segregation has been considered at a scale comparable to the interparticle distance to explain the origin of striped states in cuprates.^{6,7}

In this work we will consider the opposite case in which the scale of the inhomogeneities is much larger than the interparticle distance. The simplest form of inhomogene-

ity is the formation of spherical drops of one phase into the other phase. This case has been pioneered by Nagaev and collaborators in the context of doped magnetic semiconductors in general and of manganites in particular.^{4,5} Related ideas have been recently presented in Refs. 3,8.

We believe that for the general understanding of the large scale inhomogeneous phase the specific mechanism producing phase separation (PS) in the absence of LRC forces is rather unessential. Of course specific short range interactions in each physical system will lead to different A and B phases (which will also depend on the doping regions one considers) giving rise to different physical situations. However, in the same spirit of the Maxwell construction, one can perform a general analysis, irrespectively of the microscopic mechanisms of PS.

We consider two charged phases A and B with a compensating rigid background and we study the drop formation in a density-driven first-order phase transition between A and B . By definition, B (forming the drops) and A (forming the surroundings) have different densities; one of the phases is undercompensated and the other is overcompensated by the background. It follows that the drops are charged and they repel each other. Since the drops are formed by many particles, quantum effects are negligible and they form a Wigner crystal of drops.

A large number of small drops minimize the Coulomb energy but cost too much surface energy. The distance between the drops and the drop radius is found by minimizing a free energy which takes into account both these effects.^{4,5}

In ordinary PS the Maxwell construction (MC) is invoked to find the range of density $n_A^0 < n < n_B^0$ in which a system prepared with the overall density n separates in two regions with densities n_A^0 and n_B^0 respectively. We generalize here the MC and derive the general equations that should be satisfied in the inhomogeneous coexistence region by the the chemical potential and the pressure of each phase (Sec. II). We solve the equations in the simple (but general enough case) in which the free energy of both the A and B phases can be approximated by a parabola (Sec. III).

Next to illustrate the generality of theses ideas we consider some applications. We discuss the stability of the electron gas and of the Wigner crystal at low density against a bubble phase (IV). We consider frustrated PS in the $t - J$ model (Sec. V) and in the Manganites (Sec. VI). We conclude with a summary of the main results (Sec. VII).

II. FREE ENERGY AND COEXISTENCE EQUATIONS

We consider a density-driven first order phase transition in the presence of the LRC interaction and surface energy. We look for the formation of a mixed state by increasing the density from the uniform A phase. The mixed state is modeled by a Wigner crystal of drops of B phase in the host phase A . The total volume of the A (B) phase and the whole system are V_A (V_B) and V respectively with $V = V_A + V_B$. The volume fraction of the B phase is $x \equiv V_B/V$. We assume that the drops are spherical. This will be a good approximation as long as x is small and the crystal field is also approximately spherical. This is true for fcc, bcc and hcp lattices.^{9,10} To compute the energy we use the Wigner-Seitz approximation.^{4,9,10} We divide the system in slightly overlapping spherical cells each one with the volume $4\pi R_c^3/3 = V/N_d$ where N_d is the number of drops and R_c is the radius of the cell. Fig. 1 shows a schematic view of the cell density profile. R_d is the radius of the drop.

First we consider the electrostatic energy. The cells are neutral (by construction) and only the charge inside the cell contributes to the electric field in the cell.

The charge density of phase B is n_B (actually $-en_B$ but we drop the charge of the particles $-e$ for simplicity). The dashed background charge density in Fig. 1 ($-n_A$) compensates the A charge density n_A , and a slice of height n_A of the B charge density. For the propose of computing the electrostatic energy these charge densities can be eliminated and one is left with the density $(n_B - n_A)$ inside the drop and $-(n - n_A)$ for the background. We will call the former “drop contribution” and

the latter the “background contribution”. There is no “host” contribution due to the above cancellation.

We are assuming that the density is constant within each phase region. In general this is not true since the phases tend to adjust their density also within each phase to make the total electrochemical potential constant. For simplicity we neglect this Volta like effect and consider a variation of the particle density only among different phases. This approximation implies also that we are neglecting the natural tendency of metals to screen electric fields. However one should keep in mind that in the mixed state, whose stability we want to analyze, the customary Thomas-Fermi screening mechanism is in general not fully effective. In fact a complete screening ($\mathbf{E} = 0$) requires a total charge in the surface of the order of the total charge of the drop Q defined below. Such enormous surface charge, which is of the order of the drop volume, cannot be realized since it requires an enormous electron kinetic energy cost. The situation is therefore quite different from the usual linear Thomas-Fermi arguments in which the total screening charge is negligible with respect to the total charge of the metal and does not affect the overall density. In our case we are in a strongly non-linear limit and total Thomas-Fermi screening is not possible. On the other hand some Volta like relaxation will occur which will tend to reduce the strength of the Coulomb forces. This will renormalize the parameters and make drops larger than our estimates but we do not expect qualitative changes in the results.

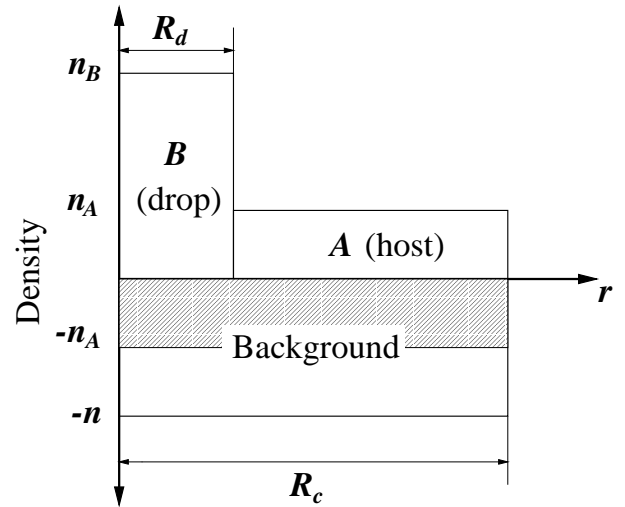


FIG. 1. Schematic view of a cell density profile with a drop of B phase in the host A . The origin is at the center of the cell. The dashed region of the background compensates the A density and part of the B density.

Another assumption is that the charge is spread uniformly and that microscopic discreetness effects can be neglected. One can see that corrections to the electrostatic energies due to discreetness are of order a^2/R_d^2

(Appendix. A) where a is the characteristic length of the microscopic structure (for example a lattice constant). Therefore they are negligible in our analysis which considers $R_d \gg a$.

With the above approximations the total electric field inside the cell is written as $\mathbf{E} = \mathbf{E}_b + \mathbf{E}_d$ where b (d) refers to the background (drop) contribution. Integrating the square of the electric field we obtain three contributions to the electrostatic energy: $\epsilon = \epsilon_d + \epsilon_b + \epsilon_{d-b}$ with

$$\epsilon_d = \frac{1}{8\pi} \int d^3 \mathbf{r} \mathbf{E}_d^2 \quad (1)$$

and a similar equation for the background. The interaction energy is

$$\epsilon_{d-b} = \frac{1}{4\pi} \int d^3 \mathbf{r} \mathbf{E}_b \cdot \mathbf{E}_d \quad (2)$$

The electric fields can be easily evaluated with Gauss theorem. One obtains

$$\epsilon_d = Q^2 \frac{3}{5R_d} \quad (3)$$

$$\epsilon_b = Q^2 \frac{3}{5R_c} \quad (4)$$

$$\epsilon_{d-b} = 3Q^2 \left(-\frac{1}{2R_c} + \frac{R_d^2}{10R_c^3} \right) \quad (5)$$

where $Q \equiv -e(n_B - n_A)v_d$ is the effective charge inside the drop. The volume of a drop is $v_d = 4\pi R_d^3/3$ and the number of drops is given by $N_d = V_B/v_d = xV/v_d$. Finally the total electrostatic energy per unit volume can be put as:

$$e_e = \frac{4\pi e^2}{5} (n_B - n_A)^2 R_d^2 x g(x) \quad (6)$$

and $g(x) = (2 - 3x^{1/3} + x)/2$. Setting one of the densities to zero one recovers the expressions obtained by Nagaev and collaborators for the particular case of a mixed state composed of an antiferromagnetic insulating phase and a ferromagnetic metallic phase.^{4,5}

The surface energy is parametrized with a quantity σ with dimensions of energy per unit surface. In general σ will be a function of the densities n_A , n_B . The total surface energy per unit volume is:

$$e_\sigma = 4\pi\sigma R_d^2 \frac{N_d}{V} = \frac{3\sigma x}{R_d} \quad (7)$$

We work at a fixed total volume V and number of particles N . At a given temperature the free energy is $F = F(V_B, N_B) + F(V_A, N_A) + V e_e + V e_\sigma$. We have to minimize this respect to R_d, V_B and N_B subject to the conditions $V_B + V_A = V$, $N_B + N_A = N$. We can work with the free energies per unit volume $f = F/V$, $f_B = F(V_B, N_B)/V_B$ and define the densities $n_B = N_B/V_B$ etc. so the function to minimize is:

$$f = (1 - x)f_A(n_A) + xf_B(n_B) + e_e + e_\sigma \quad (8)$$

The constraint in the number of particles is written as $n = xn_B + (1 - x)n_A$ and the constraint in the volume is satisfied by putting $V_B/V = 1 - x$. It is convenient to define $\delta = n_B - n_A$ and to use the constraint in the number of particles to eliminate n_B and n_A in favor of n and δ . Minimizing respect to R_d , δ and x one obtains:

$$R_d = \frac{1}{2} \left(\frac{15\sigma}{\pi g(x) e^2 \delta^2} \right)^{1/3} \quad (9)$$

$$\mu_B - \mu_A = -\frac{8\pi e^2 R_d^2 \delta g(x)}{5(1 - x)} \quad (10)$$

$$+ \frac{3}{R_d} \left(\frac{x}{1 - x} \frac{\partial \sigma}{\partial n_A} - \frac{\partial \sigma}{\partial n_B} \right) \quad (11)$$

$$p_B - p_A = (\mu_B - \mu_A)[n + \delta(1 - 2x)] \quad (11)$$

$$+ \frac{4\pi}{5} e^2 \delta^2 R_d^2 (1 - 2x^{1/3} + x) \quad (11)$$

$$+ \frac{3}{R_d} \left[\sigma - x\delta \left(\frac{\partial \sigma}{\partial n_A} + \frac{\partial \sigma}{\partial n_B} \right) \right]. \quad (11)$$

Here p_B, p_A (μ_B, μ_A) are the “intrinsic” pressures (chemical potentials) of each phase respectively. The word “intrinsic” stands for the values of these quantities in the presence of a fictitious fully compensating background, in other words they refer to a uniform single-phase situation. Mathematically $\mu_A = \partial f_A / \partial n_A$, $p_A = -f_A + \mu_A n_A$, etc. Equations (10)-(11) determine the jump in these quantities at the interface in order to have thermodynamic equilibrium when long range effects due to inhomogeneities are present.

The effect of the long range forces and of the surface energy in the jumps is easy to understand. Let us neglect for simplicity the density dependence of the surface energy ($\partial \sigma / \partial n_A = \partial \sigma / \partial n_B = 0$). Due to the different charge distributions, the electrostatic potential energy $-e\phi$ of an electron inside and outside the drops is different. In equilibrium this jump in the electrostatic potential [Eq. (10)] should be compensated by a jump of the intrinsic chemical potentials to make the electrochemical potential constant in the whole system. For $\delta > 0$ the drop repels electrons so the electrostatic potential energy will be lower outside the drop i.e. $-e\phi_A < -e\phi_B$. The intrinsic chemical potential outside will have to be larger than inside as the sign in the first term of Eq. (10) implies.

Regarding the pressure, in equilibrium the intrinsic pressure inside the drop, p_B , should equal the pressure exerted by the host p_A plus the pressure exerted by the surface $3\sigma/R_d$ plus an electrostatic contribution given by the first two terms in Eq. (11). The surface tension tends to increase the pressure inside the drop since it tends to reduce the area of the surface. For small $\delta > 0$ instead the electrostatic force induces a contribution with the opposite sign since an increase in the drop volume at constant particle number decreases the difference in densities between the interior and the exterior of the drop

and hence the Coulomb cost. This effect is given by the term $(\mu_B - \mu_A)n$ in Eq. (11). For larger δ selfenergy effects ($\propto \delta^2$) enter into play.

In the limit $e \rightarrow 0$ the radius goes to infinity with $R_d^2 e^2 \rightarrow 0$ and one gets $\mu_B = \mu_A = \mu$ and $p_A = p_B = p$ i.e. $\mu\delta = f_B - f_A$ which are the conditions for MC.

III. GENERAL ANALYSIS OF THE DROP SOLUTION

In this section we set up the basic ideas for the drop solution in the general case of a first order phase transition in which each phase corresponds to a local minimum of the free energy which we model with a parabola. For simplicity we assume that the surface tension is density independent. Without loss of generality we write the parabolas for the free energies of each phase as a quadratic expansion around the MC densities:

$$\begin{aligned} f_A(n_A) &= f_A^0 + \mu^0(n_A - n_A^0) + \frac{1}{2k_A}(n_A - n_A^0)^2 \\ f_B(n_B) &= f_B^0 + \mu^0(n_B - n_B^0) + \frac{1}{2k_B}(n_B - n_B^0)^2 \end{aligned} \quad (12)$$

The quantities with the “0” superscript (or subscript below) satisfy MC in the absence of LRC forces i.e. $f_B^0 - f_A^0 = \mu^0\delta_0$ and $\delta_0 = n_B^0 - n_A^0$. The linear sloop μ^0 is the same for the two phases due to the MC condition. The MC density n_0 and the volume fraction are related by $n_0 = n_A^0 + \delta_0 x$. Our aim here is to obtain the equations which control the deviation from MC behavior.

We define a dimensionless global density

$$n' \equiv (n - n_A^0)/\delta_0$$

which measures the distance from the point in which the B phase appears in the absence of Coulomb forces. In MC the coexistence region is given by $0 < n' < 1$.

Eqs. (9)-(11) determine δ , R_d and x for a fixed density where now μ_A , μ_B , p_A , and p_B can be expressed in terms of the parameters appearing in Eqs. (12).

In practice it is much easier to solve the equations by fixing the volume fraction x and solving for δ , R_d and n , i.e. we find which density one should put in the system to obtain a mixed state with a given volume fraction. This is because the solutions happen to be multivalued functions of n whereas they are single valued functions of x (see below).

For a fixed volume fraction x we define the dimensionless density deviations from the MC values: $\hat{n} = (n - n_0)/\delta_0$ and $\hat{\delta} = (\delta - \delta_0)/\delta_0$. The density deviation \hat{n} measures the shift in the global density needed to have the same volume fraction of a system without LRC interaction.

The theory has two dimensionless parameters. One is the ration k_B/k_A . The other measures the strength of

the LRC interaction and of the surface energy effects and is given by:

$$\lambda = 2 \frac{k_m}{\delta_0} \left(\frac{9\pi e^2 \sigma^2}{5\delta_0} \right)^{1/3} \quad (13)$$

where $k_m = \max(k_A, k_B)$. Notice that δ_0 measures the separation in density of the vertices of the two parabolas in Eq. (12). The larger is δ_0 , the larger is the energy gain of the MC phase separated state respect to the uniform state. λ characterizes the competition and the relative weight of the LRC and surface energy cost and the energy gain in the MC. The coupling constant goes to zero as $e \rightarrow 0$ with σ finite. This correspond to the usual PS. The case $\sigma \rightarrow 0$ with finite e correspond to an infinite number of drops of zero radius. In this maximum intermixing situation the charges of the two phases spatially coincide and the Coulomb cost goes also to zero so that the MC is again valid. Notice however that this last idealized situation cannot be reached in practice because at some point for small drop radius the continuous approximation will fail.

Eliminating the radius in Eqs. (9)-(11) and from the explicit expressions [Eqs. (12)] of f_A and f_B we obtain the following equations for the density deviations:

$$\begin{aligned} \hat{n} \left(\frac{1}{k_B} - \frac{1}{k_A} \right) + \hat{\delta} \left(\frac{1-x}{k_B} + \frac{x}{k_A} \right) = \\ - \frac{\lambda}{k_m(1-x)} \left[\frac{g(x)}{(1+\hat{\delta})} \right]^{1/3} \end{aligned} \quad (14)$$

$$\begin{aligned} - \frac{\hat{n}}{k_A} + \frac{x\hat{\delta}}{k_A} + \hat{n}\hat{\delta}(1-x) \left(\frac{1}{k_B} - \frac{1}{k_A} \right) + \frac{1}{2}\hat{n}^2 \left(\frac{1}{k_B} - \frac{1}{k_A} \right) + \\ \frac{\hat{\delta}^2}{2} \left[\frac{1-2x}{k_B} + \frac{2x}{k_A} + \left(\frac{1}{k_B} - \frac{1}{k_A} \right) x^2 \right] = \\ - \frac{3\lambda j(x)}{2k_m} (1+\hat{\delta})^{2/3} \end{aligned}$$

where

$$j(x) = \frac{\left(1 - x^{\frac{1}{3}}\right)^2 \left(3 + 4x^{\frac{1}{3}} + 3x^{\frac{2}{3}} + x\right)}{3 \left(1 + x^{\frac{1}{3}} + x^{\frac{2}{3}}\right) g(x)^{\frac{2}{3}}}$$

Eqs. (14) can be solved numerically for general values of the parameters. For small LRC force we can linearize the equations expanding for small λ . We get:

$$\hat{n} \left(\frac{1}{k_B} - \frac{1}{k_A} \right) + \hat{\delta} \left(\frac{1-x}{k_B} + \frac{x}{k_A} \right) = - \frac{\lambda g(x)^{1/3}}{k_m(1-x)} \quad (15)$$

$$- \frac{\hat{n}}{k_A} + \frac{x\hat{\delta}}{k_A} = - \frac{3\lambda j(x)}{2k_m} \quad (16)$$

For the sake of simplicity in the following we will consider the linearized solution. We checked that for all the

physical properties the difference between the linearized and the exact solution is quite small in the range of λ where the drop solution is stable.

The linearized solution takes a simple form when written in the original variables:

$$\begin{aligned} n_A &= n_A^0 + \frac{3}{2} \lambda \delta_0 \frac{k_A}{k_m} j(x) \\ n_B &= n_B^0 + \frac{3}{2} \lambda \delta_0 \frac{k_B}{k_m} h(x) \end{aligned} \quad (17)$$

where $h(x) = j(x) - 2g(x)^{1/3}/[3(1-x)]$.

In the case of $\lambda = 0$, according to MC, the system separates in two phases with densities n_A^0 , n_B^0 respectively independently of the volume fraction. For nonzero λ and small x the B phase divides in drops and the density in each phase depends on the volume fraction of B phase. The deviation of each density from MC prediction is proportional to λ and to the compressibility of each phase. Notice that the density of an incompressible phase does not depend on the volume fraction even in the presence of LRC forces.

In Fig. 2 we show the behavior of the two functions which determine the dependence of the densities on the volume fraction. For small x both n_A and n_B tend to be larger than in the MC case. In fact we will see below that the global density n' to find PS is larger than the one for $\lambda = 0$.

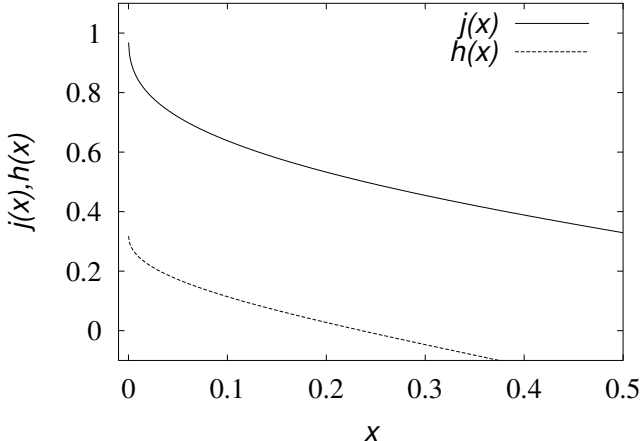


FIG. 2. The dimensionless functions that determine the change in n_A (upper curve) and n_B (lower curve) for small λ vs. the volume fraction x . [See Eq. (17)]

We are interested in the behavior of these quantities for a given global density n' , our true control variable, rather than as a function of the volume fraction. We need hence the volume fraction as a function of the global density n' . From the solution of the linearized equations we find:

$$n' = x + \frac{3}{2} \lambda \left[(1-x) j(x) \frac{k_A}{k_m} + x h(x) \frac{k_B}{k_m} \right] \quad (18)$$

The inverse of this function gives the volume fraction as a function of the density.

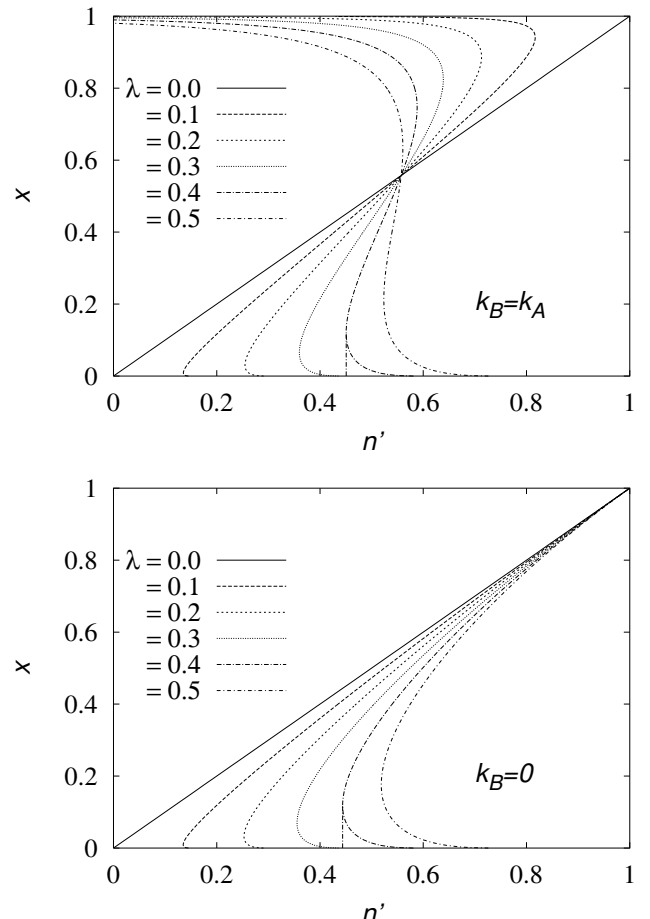


FIG. 3. Top panel: Volume fraction vs. n' for (from left to right at the bottom) $\lambda = 0, 0.1, 0.2, 0.3, 0.4, 0.5$ and $k_B = k_A$. For $\lambda = 0.4$ we indicate with a vertical line the discontinuity in the volume fraction to go from the uniform solution to the drop solution by increasing the density. Bottom panel: Same for $k_B = 0$. The approximations done are rigorously valid only for small x .

Another important quantity is the drop radius. Inserting the solution of the linearized equations in Eq. (9) we find:

$$R_d = \frac{3l}{\lambda g(x)^{\frac{1}{3}} \left(1 + \frac{3\lambda(k_B h(x) - k_A j(x))}{2k_m} \right)^{\frac{2}{3}}} \quad (19)$$

where the basic length unit in the theory is given by $l = k_m \sigma \delta_0^2$. From the definition of the volume fraction one finds that the cell radius is given by $R_c = R_d / x^{1/3}$.

In the following we analyze in detail the two cases: i) the compressibilities of the two phases are equal ($k_B = k_A = k_m$) and ii) one of the compressibilities is zero.

In Fig. 3 we plot the volume fraction as a function of global density from Eq. (18). The volume fraction is a multivalued function of n' and in the case $k_B = k_A$ has a lower branch close to $x = 0$, an intermediate branch, and an upper branch close to $x = 1$. The intermediate branch is the physical solution. This will be shown below by looking at the free energy in each branch. The physical solution has the intuitive property that the volume fraction increases as global density increases.

We see that the bifurcation density n'_{bif} at which the phase separated solution appears for finite λ is larger than in MC. On the other hand the B phase appears with a finite volume fraction and its growing rate is larger than in the MC case. Interestingly both the volume fraction at the bifurcation point and the bifurcation density n'_{bif} are almost the same for $k_B = k_A$ and for $k_B = 0$ and depend only on λ as can be seen by comparing the two panels in Fig. 3.

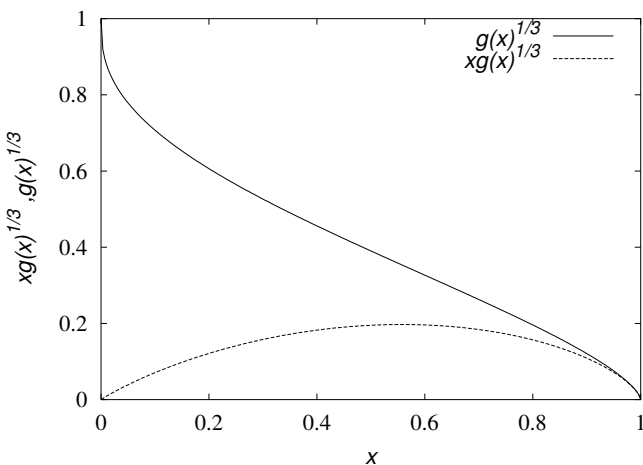


FIG. 4. The functions $g(x)^{1/3}$ and $xg(x)^{1/3}$ that control the dependence of the drop energy on the volume fraction.

Notice that the spheric drop solution is strictly valid only for small x since we are assuming drops of B phase in A . Close to $x = 1$ the opposite situation will make sense. Furthermore we are assuming a spherical lattice crystal potential which will not be true close to $x = 1/2$. An improved treatment approaching $x \sim 1/2$ should allow for drops of arbitrary shape in the lattice crystal potential. In practice, however, our approximations can be meaningful even at intermediate and large x . In fact the exact solution for a given value of k_A and k_B is related by symmetry to the solutions obtained by exchange of k_A and k_B in the following way. The curve $x(n')$ for one set of compressibilities should be equal to the curve $x(n')$ for the other set rotated 180 degrees. It follows that for the case $k_B = k_A$ the exact solution should have inversion symmetry around the point $(x, n') = (1/2, 1/2)$. This holds approximately in the present treatment which can therefore be considered qualitatively correct for all x . Hav-

ing this in mind we show the curves for the whole range of x . We have also checked that our approximate solution for $k_A = 0$ is very similar to the one for $k_B = 0$ (Fig. 3) rotated 180 degrees.

The fact that the theory is well behaved for $x \rightarrow 1$ can be traced back to the fact the electrostatic energy Eq. (6) correctly cancels in this limit and the whole drop energy [the last two terms in Eq. (8)] gives an approximately symmetric contribution once the drop radius has been eliminated:

$$e_d \equiv e_e + e_\sigma = 3 \left(\frac{9\pi}{5} \right)^{1/3} (\sigma e \delta)^{2/3} x g(x)^{1/3} \quad (20)$$

This can be seen in Fig. 4 where we plot the function $xg(x)^{1/3}$.

In the case $k_B = 0$ the constraint between the volume fraction and the densities and the fact that the B density is fixed makes all the curves to converge to the MC case when $x \rightarrow 1$ as shown in Fig. 3. The same happens when $k_A = 0$ and $x \rightarrow 0$.

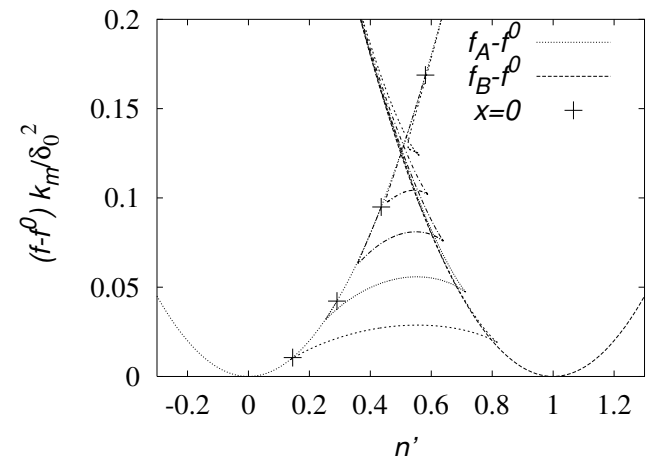


FIG. 5. $f_A - f^0$, $f_B - f^0$, and $f - f^0$ in the drop solution for $\lambda = 0.1, 0.2, 0.3, 0.4, 0.5$ (from bottom to top) and $k_B = k_A$ vs. n' . Here $f^0(n')$ is the MC free energy for $\lambda = 0$ (a straight line). The cross indicates the value with $x = 0$ of the drop solution for each λ .

To decide the stability of the solution we have to compare the drop solution with the single phase solution. In Fig. 5 we show $f_A(n')$, $f_B(n')$ with $k_B = k_A$ for various λ . The MC line $f^0(n') = f_A^0 + n'(f_B^0 - f_A^0)$ has been subtracted. The energy also is a multivalued function of n' . As the density increases the drop solution appears at n'_{bif} with two different branches. In the upper (unstable) branch x decreases with density till the point $x = 0$ highlighted with a cross in Fig. 5. For the lower branch one finds the expected behavior i.e. x increases with density. The upper branch is almost degenerate with the bulk $f_A(n)$ free energy. Near the bifurcation the three

solutions (homogeneous, drop stable and drop unstable) are very close in energy. Approximation in the solution of the Eq. (14) can lead to wrong conclusions about the relative stability. In this case one has to refer to the non-linearized solution. For the latter (not shown) we find that the bifurcation density n_{bif} is lower than the density n_c at which the energy of the lower energy drop solution crosses the energy of the uniform phase $f_A(n')$. However the difference between n_c and n_{bif} is negligible for all practical proposes except for the largest λ . In this case there is a small region ($\lambda_c = 0.49 < \lambda < 0.57$) in which the lower energy drop solution still exist but is less stable than the homogeneous solution. If we neglect this small effect the phase diagram of the drop solution is given by n_{bif} vs. λ . This is shown in Fig. 6.

The uniform-drop boundary line is determined by the condition $\partial n'/\partial x = 0$ (see Fig. 3). For $\lambda > \lambda_c$ the homogeneous solution is stable for any global density. The uniform A-B boundary line is determined by the crossings of the parabolas in Fig. 5.

When one of the compressibilities goes to zero, say k_B , the crossing moves to the right in Fig. 5 and the uniform B region shrinks until the boundary line for uniform B phase approaches the MC value ($n = n_B^0$). At the same time λ_c increases. Analogous results are obtain for k_A going to zero.

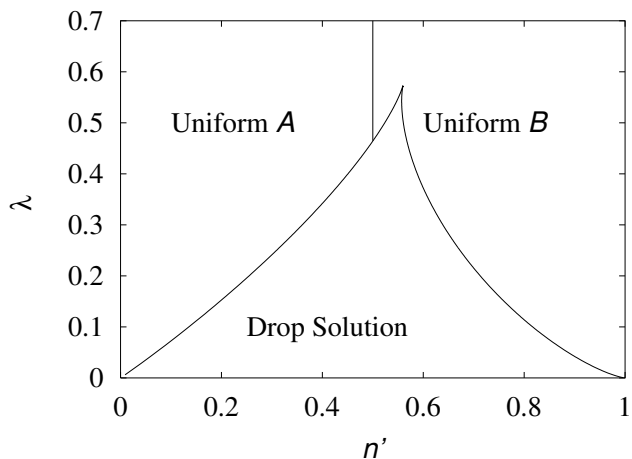


FIG. 6. Locus of existence of the low-energy drop solution in the λ - n' plane for $k_A = k_B$. This almost coincides with the phase diagram in the sense that when the drop solution exist it is more stable than the uniform solution except close to $\lambda = 0.5$ and in a very narrow region around the drop-uniform boundary line (see text).

In the upper panel of Fig. 7 we show the density of each phase as a function of the global densities for $k_B = k_A$. Increasing the global density the transition occurs from the uniform A phase, with density higher than the MC one, to the drop state. In the MC case the density of the A phase is continuous at the transition and remains

constant in the coexistence region. For nonzero λ the A phase density has a discontinuity when the drops occur. Remarkably both local densities decrease as the global density increases. This behavior can be understood more easily by looking at the $k_A = 0$ limit. The corresponding densities are shown in the lower panel of Fig. 7. The lower curves for n_A shrink to the MC case and the upper curves for n_B remain very similar (even quantitatively) except close to $n' \rightarrow 0$. We mention that in the case $k_B = 0$ (not shown) a similar effect is seen exchanging A with B.

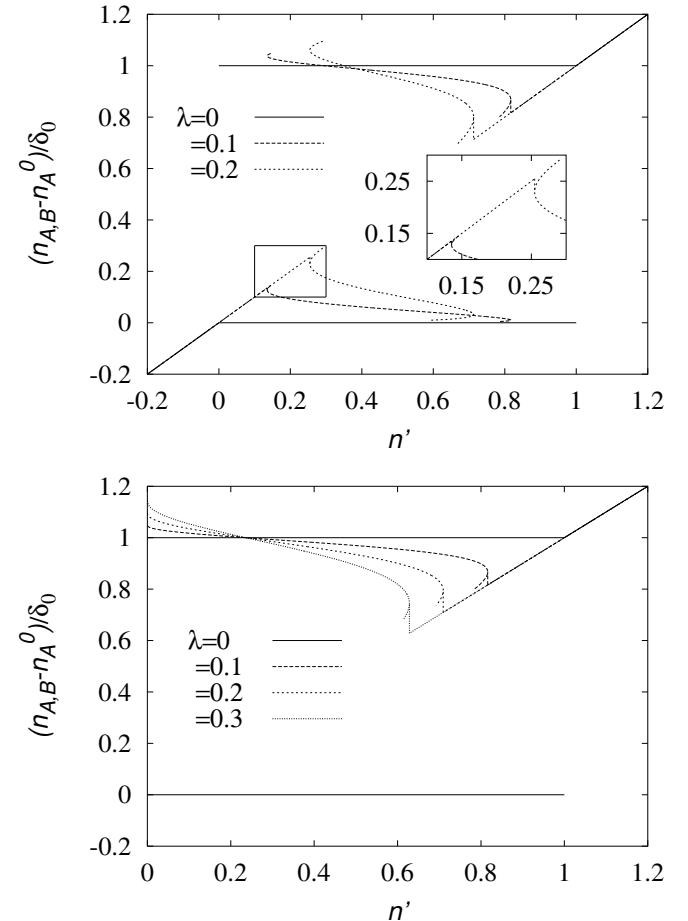


FIG. 7. Normalized densities of each phase as a function of normalized global density n' for different λ . The upper panel is for $k_B = k_A$ and the lower panel is for $k_A = 0$. For each panel the lower curves correspond to the A phase and the upper curves to the B phase. In the coexistence region multivalued densities appear. The long brunch is the physical one and the short branches are unphysical. The inset shows an enlargement of the A density to resolve the discontinuities.

For $k_A = 0$ we have a compressible phase growing in an incompressible phase. This simplifies the physics because the A density is fixed and the B density is not any more bivaluated for small densities.

To fix ideas we will call the B phase a “metal” and the

A phase the “vacuum”. Accordingly we put $n_A = n_A^0 = 0$ and $f_A = 0$. These last conditions do not change the solution but make the interpretation more transparent.

The total free energy can be put as:

$$f = x \left[f_B^0 + \mu^0 (n_B - n_B^0) + \frac{(n_B - n_B^0)^2}{2k_m} + e_d/x \right]$$

where the first three terms in the brackets are the B free energy and the last term is the drop energy [Eq. 20] divided by the volume fraction. In this simple case e_d/x can be thought as a correction to the free energy of the metal. $e_d/x \propto g(x)^{1/3}$ was plotted in Fig. 4 as a function of volume fraction. We see that the drop correction is larger when the drops have a small volume fraction and then decrease monotonously as the cell is transformed from vacuum to a uniform metal.

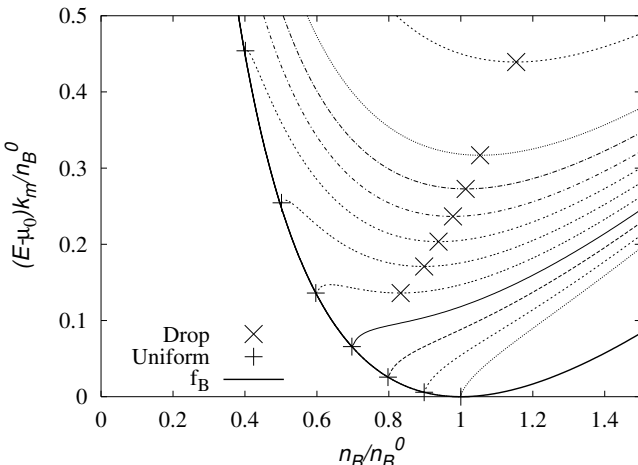


FIG. 8. Normalized energy per particle as a function of n_B/n_B^0 for $\lambda = 0.3$. The thick line correspond the uniform phase and the thin lines to the drop state with n' changing from zero (top) to one (bottom) in steps of 0.1. The crosses indicate the drop solution and the uniform solution.

In the MC case the n_B density is kept fixed, $n_B = n_B^0$, and the volume fraction increase linearly with the density accordingly to the constraint $x = n/n_B$. In the presence of LRC and surface energies, due to the fact that e_d/x decrease with x it is convenient for the system to make the n_B density to decrease so that the volume fraction grows faster and the drop cost is reduced. In other words as the density grows drops tend to expand at the expense of the vacuum volume by a larger amount than what MC would predict. The superlinear increase of the volume fraction can also be seen by looking at the up right corner of the the lower panel of Fig. 3 (up side down) according to the approximate inversion symmetry discussed above.

Mathematically this effect can be seen by using the constraint to eliminate the volume fraction in favor of n_B . The free energy reads now $f = nE$ where E is the energy per unit particle and is given by:

$$E - \mu^0 = \frac{n_B^0}{k_m} \left[\frac{(n_B - n_B^0)^2}{2n_B n_B^0} + \frac{3}{2} \lambda \left(\frac{n_B^0}{n_B} \right)^{1/3} g(n/n_B)^{1/3} \right] \quad (21)$$

The f_0^B term has been eliminated with the MC condition. The equilibrium density is found by minimizing Eq. (21) with respect to n_B . In Fig. 8 we show $E - \mu^0$ as a function of n_B for $\lambda = 0.3$ and different values of n' . The thick line is the energy of the uniform metal [the first term in the brackets in Eq. (21)] and is minimized at the MC density.

For very small n the geometric factor $g^{1/3} \sim 1$ and the drop contribution goes as $1/n_B^{1/3}$. This shifts the minimum to larger values of the density as can be seen from the upper curves of Fig. 8 where the energy per particle is given for various values of the global density and $\lambda = 0.3$. This explain the behavior of the n_B density in the limit $n' \rightarrow 0$ (Fig. 7). As the density increases the density dependence of $g^{1/3}$ cannot be neglected any more. This factor tends to reduce the minimum to lower densities according to the above discussion. Above $n' \sim 0.6$ the uniform solution becomes more favorable (see also Fig. 7). Notice that the density is well below the MC value for a uniform solution ($n' = 1$). This shows the effect of the LRC interaction stabilizing a uniform solution.

In the case $k_A = k_B$ the same physics applies for n_B . As is obvious from symmetry considerations the argument can be reverted to explain the decrease of n_A with increasing densities.

It is important to remark that the whole behavior can change if the surface energy σ had a strong density dependence. For this reason the interpretation of the B phase as a metal should be taken with caution since in general in a metal the surface energy will depend strongly on density. Specific examples will be treated below.

In Fig. 9 we show the drop radius as a function of density from Eqs. (18),(19) for $k_B = k_A$. R_d diverges as $\lambda \rightarrow 0$ [cf. Eq. (19)] indicating that MC can be realized with a single large drop of B phase in A . As λ increases the initial drop radius $R_d(n'_{\text{bif}})$ decreases. By increasing n' at fixed λ , the radius increases together with the increase of the B phase.

Another peculiarity of the curves in Fig. 5 is that the free energy of the drop solution has the “wrong” curvature, that is the compressibility (defined from $\partial^2 f / \partial^2 n$) is negative. This does not necessarily imply an instability since the usual stability condition of positive compressibility is formulated for a neutral system, that is including the background compressibility. Since we are assuming the inverse background compressibility to be an infinite positive number (in our analysis the background density has a fixed homogeneous value) it follows that the total compressibility is positive and from this point of view the system is in a stable mixed state. Of course this does not guarantee stability against more complicated solutions than the simple crystal of drops.

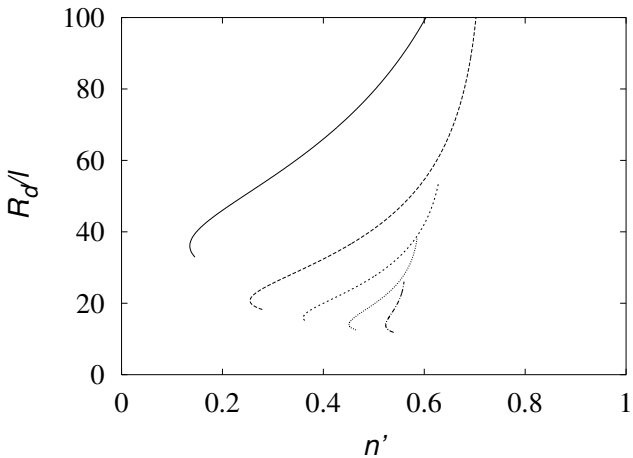


FIG. 9. Drops radius in units of length l defined after Eq. (19) for $\lambda = 0.1, 0.2, 0.3, 0.4, 0.5$ vs. n' (from top to bottom). For each curve the upper branch is the stable one.

The situation is more severe for $\lambda > \lambda_c$ where the drop solution, if it exists, is not stable. In this case, the system remains always single phase and the free energy is given by the branches of the parabola with the smaller energy in Fig. 5. It changes suddenly from A phase to B phase at the density n'_c for which $f_A(n'_c) = f_B(n'_c)$. (For our parameters $n'_c = 0.5$). The problem is now that the energy has a cusp pointing upwards at n'_c which implies an infinite negative inverse compressibility. This will compete with the infinite positive inverse compressibility of the background. Clearly one should consider in this case the background compressibility (e.g. the lattice compressibility) since the beginning. As a first step we can add to the above electronic free energy a background free energy contribution $f_b(n) = (n - n_c)^2/2k_b$. A very rigid (but not infinitely rigid) background is described by a very small $k_b > 0$ which correspond to a very narrow parabola for the background free energy. The total free energy, background plus cusp, will have a cusp pointing up with two local minima nearby. Since now the total free energy corresponds to a truly neutral system one can make a MC between the two local minima. One obtains a phase separation between A and B with the background adjusting its density in each region to the density of each phase to make it neutral. The same argument applies at the critical density where the drop solution crosses the uniform solution, although the negative dip is much less pronounced in that case. This scenario implies a solubility limit for the dopants with a forbidden region of the overall density. Usually the electronic system is a crystal where the background is provided by the ionic lattice. If one tries to prepare the crystal in the forbidden density region it will brake in two pieces each one with a different lattice constant. This may provide a mechanism to explain why some real materials are so difficult to dope in certain doping ranges.

Since the electronic free energies depend on external parameters, a remarkable implication is that the forbidden doping region will also depend on external parameters like magnetic field, temperature, pressure, etc. In other words a crystal can be driven from a single phase to a two phase situation by changing external parameters. This is very reminiscent of the situation in some manganites where one finds that a single phase crystal brakes in a multidomain crystal by lowering the temperature. The multidomain system shows lattice mismatch and large stress at the interfaces.^{11,18}

In the following sections we apply to different physical systems the ideas developed in this section.

IV. STABILITY OF THE JELLIUM MODEL

Here we discuss the case of a system of electrons in a uniform rigid background usually called the “jellium” model. Although we find that drops do not form in this case, this first discussion is very useful to illustrate the range of applicability of the present ideas.

The problem is the following: It is well known that a low density electron gas has a negative electronic compressibility.¹⁰ Will this lead to drop formation?

To describe in an approximate way the electronic energy one can use the Wigner interpolation formula for the correlation energy. In this approximation the ground state energy per particle at zero temperature is given by:¹⁰

$$E_{el}/Ry = \frac{2.2099}{r_s^2} - \frac{0.9163}{r_s} - \frac{0.88}{r_s + 7.8} \quad (22)$$

where the first term is the kinetic energy, the second term is the exchange energy, and the last term is the correlation energy. Here $r_s = [3/(4\pi n)]^{1/3}/a_0$ and a_0 is Bohr’s radius.

The energy per unit volume is $f_{el}(n) = E_{el}n$. In Fig. 10 we plot f_{el} and E_{el} as a function of density. These curves can be interpreted in two different ways. If the background compressibility is given only by the electrostatic self energy (already included) then the curves represent the total energy of the system, background plus electrons. We call this the compressible background case. Two different criteria give thermodynamic instability for the compressible background case. First for $na_0^3 < 0.0015$ (up arrow) the compressibility is negative. More importantly for $na_0^3 < 0.003 \equiv n_{el}^0$ (down arrow) the pressure is negative. The latter means that if the system is prepared with a density lower than n_{el}^0 , then electrons and background will relax to a self bound system with a lower volume and $n = n_{el}^0$ (from now on we shall measure densities in units of Bohr inverse volume a_0^3). We can consider this result as due to the MC of phase separation between the electronic system+background and the vacuum. In fact it is easy to see that $n = n_{el}^0$ satisfy a MC in which

the MC line intersects the origin. By putting an external pressure densities higher than n_{el}^0 become physically accessible. The values of $n = n_{el}^0$ can change when more accurate forms of the correlation energy are considered but the qualitative picture will remain the same.

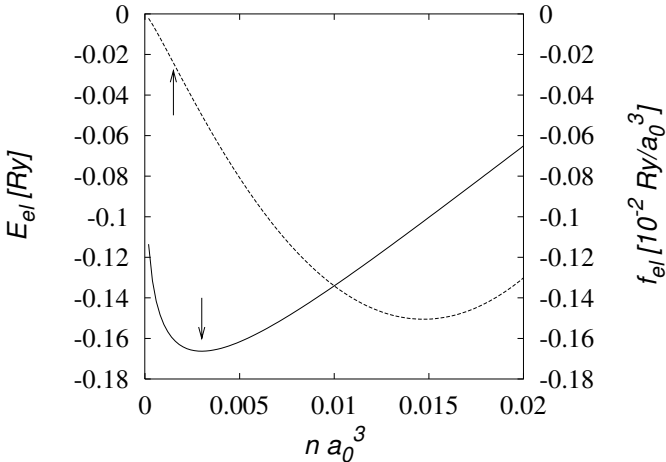


FIG. 10. Energy per particle (left axis, solid line) and per unit volume (right axis, dashed line) as a function of density obtained from Wigner interpolation formula. The vertical arrows indicate the density at which the pressure is zero (lower one) and the density at which the jellium model contribution to the compressibility becomes zero (upper one). In the latter case the corresponding change of curvature is almost indistinguishable to the bare eye.

The above interpretation is not useful in real situations where forces other than the electrostatic one can constrain the background to have a certain density. This leads to a second interpretation of the curves in Fig. 10. Since the background has an additional non-electrostatic contributions to the compressibility (for example coming from core-core repulsion of the atoms), the plots of Fig. 10 are not any more the total energy of the (neutral) system as function of density.

A simple hypothesis to describe such a system is to assume in the model that the substrate is completely rigid. We call this the incompressible background case. Now the total density is fixed at some value and the compressibility of the whole system is infinite and the above instability criteria do not apply any more. This however does not guarantee the stability of the system. One can imagine that the system may be unstable towards an inhomogeneous phase with electron rich and electron poor bubbles in the uniform fixed background.

We analyze below the case in which the electron poor regions have zero electron density. In principle we can work as above with a quadratic expansion of the free energy around the MC case however the free energy has now a simple form which can be dealt with analytically.

A. Electron drops in background

The compressible background case suggests that the system has the tendency to separate in electron rich regions and regions of zero electron density. We will take the *A* phase to be the background with no electrons and the *B* phase to be the background with an undercompensated density of electrons. Consider first the case of low densities for the *B* phase. We can take for the bulk drop free energy the energy of a classical Wigner crystal i.e. the leading $1/r_s$ term in Eq. (22) for large r_s . This microscopic Wigner crystal should not be confused with the mesoscopic Wigner crystal that the drops would form.

It is instructive to write the free energy in the following way:

$$f = \frac{2\pi e^2}{5} n [-3n_{el}r_{el}^2 + 6n_{el}R_d^2 g(n/n_{el})] \quad (23)$$

The volume fraction has been eliminated by using the constraint in the density given by $n = xn_{el}$ where $n_{el} \equiv 3/(4\pi r_{el}^3) \equiv n_B$ and $n_A = 0$. The first term in the brackets comes from the classical Wigner crystal contribution (the leading term in $f_B \equiv f_{el}$ at low density) and the second term is the bubble contribution. The latter contains already the electrostatic bubble contribution and the surface energy contribution [Eqs. (6),(7)]. $R_d \equiv R_d(n, n_{el}, \sigma)$ is the drop radius that satisfy Eq. (9) i.e. the minimization respect to the radius has already been done.

Notice that the drop of electrons is not neutral since the density of electrons is larger than the compensating background i.e. within the drops we are dealing with a charged Wigner crystal of electrons in contrast with the usual neutral Wigner crystal of electrons. On the other hand in the computation of the charging energies of the drops [Eq. (6)] we have assumed for simplicity that the density is uniform inside the drop. In the appendix A we compute the correction to the electrostatic energy [Eq. (A1)] due to the non uniform electronic density at the microscopic scale as it should be for a charged Wigner crystal and conclude that this only changes numerical factors, which are not important for the present analysis.

Since the drop radius has already been minimized one is left with the density inside the drops (or equivalently with r_{el}) to be minimized. R_d depends on density explicitly and indirectly on $\sigma(n_{el})$. If the term $n_{el}R_d^2 g(n/n_{el})$ grows with the density faster than $n_{el}r_{el}^2$, the minimum occurs at $n_{el} \rightarrow n$ i.e. $x = 1$. This corresponds to the uniform case. If instead $n_{el}r_{el}^2$ grows faster one finds a solution with $n_{el} \rightarrow \infty$, $g \rightarrow 1$ and clearly $r_{el} > R_d$. In this case the mesoscopic bubble model is clearly not adequate. In order for both term to balance exactly one finds that the surface energy has to fulfill the relation $\sigma \sim e^2 n_{el}^{2/3} / r_{el}$. If one estimates the surface energy as a characteristic energy density $(n_{el}e^2/r_{el})$ times a characteristic length ($r_{el} \sim n_{el}^{-1/3}$) one can conclude on dimen-

sional arguments that this surface energy is precisely the one of a Wigner crystal. Smaller surface energies give drops which are too small for the mesoscopic treatment and larger surface energies give no drops at all.

What about the other contributions to the bulk free energy in Eq. (22) which will become important as the density inside the drop becomes large? They only make the drop bulk term less negative so an even smaller value of the drop radius is needed to stabilize the drop solution. From this point of view we can conclude that mesoscopic or macroscopic drops of electron gas are not possible.

The only dubious case could be close to $x = 1$ ($n_{el} \rightarrow n$). Since in this case g can be very small in principle one can have large drops without paying too much surface and electrostatic energy. However in this region Eq. (23) is not strictly valid since the volume fraction is close to 1 and one has to consider the reverse case as done below.

B. Drops of empty background

We consider the possibility of formation of drops of zero electronic density hosted by electron rich regions with density n_{el} .

We look again to the limit of the classical Wigner crystal. Now x will represent the fraction of empty electronic volume. The constraint in the density is given by $n = (1 - x)n_{el}$ and the free energy reads:

$$f = \frac{2\pi e^2}{5} [-3n n_{el} r_{el}^2 + 6(n_{el} - n)n_{el} R_d^2 g(1 - n/n_{el})]$$

We see that if $n_{el} \rightarrow n$ we can get $R_d \gg r_{el}$ with a small surface and electrostatic energy (the last term in the brackets). Using the density constraint to eliminate n_{el} in favor of x we find that for small x the free energy behaves as $n^2(-5r_0^2 + 6R_d^2)x$ with r_0 given by $n \equiv 3/(4\pi r_0^3)$. Clearly to have a minimum for small $x > 0$ we need $R_d < r_0$ and the model does not apply. The full expression for the free energy taking into account the electron kinetic energy gives an even smaller slope for the dependence of f on x so that an even smaller drop radius is obtained. We could still have drops with a finite electronic densities in both the drop and the host phases. In this way one can reduce the drop energy because it is proportional to δ^2 . One could expect to find a solution close to the critical density for zero pressure n_{el}^0 . We have searched for such a solution assuming $E_{el} \sim (n - n_{el}^0)^2$. It has higher energy than the uniform solution.

We can conclude that a 3d electron-jellium model is not unstable towards mesoscopic or macroscopic drop formation. This shows that the apparent instabilities exhibited by the low density electron gas have no dramatic consequences. Our result stems from the fact that both the energy gain coming from the MC and the energy cost have the same electrostatic origin. Of course we cannot discard instabilities that can occur at a microscopic scale.

V. FRUSTRATED PHASE SEPARATION IN THE 3D $t - J$ MODEL.

In the last few years it has become clear that many of the strongly correlated models used to describe high temperature superconductors exhibits PS in some regions of parameter space^{1,2}. Due to the strong anisotropy of these materials usually two dimensional (2d) models are considered. In this section we apply the idea of a Wigner crystal of drops to PS in models of strongly correlated electrons on a lattice. We will consider, for simplicity and homogeneity with the other sections of the paper, isotropic 3d lattice models. We expect however that the results will remain qualitative valid even for anisotropic models. Needless to say that the 3d models are interesting on its own right given the large class of strongly correlated materials where anisotropy is not important like doped C_{60} , magnetoresistant manganites, etc.

Usually in strongly correlated lattice models the Coulomb interaction is truncated to a distance of a few lattice sites and often only the on-site Hubbard U term is kept. The underlying assumption is that in a uniform ground state most of the interesting physics is governed by the short range interactions and that the effect of the long range interactions can be absorbed in the Madelung potential through a proper Hartree renormalization of the on-site energies. However in a non uniform ground state the long range part of the interaction has an important role even at the Hartree level. A simple way to take this into account is to maintain the relevant short range interactions (e.g. the Hubbard U), to evaluate the energy of the intrinsic A or B phases and to add the electrostatic and surface contribution of the drops to the total free energy. This means that we are still neglecting the Coulomb interaction at distances larger than the lattice constant a , as in the usual Hubbard model but we keep the Coulomb repulsion for mesoscopic distances of the order of the inhomogeneity scale. In other words in the Fourier transform of the Coulomb potential, $4\pi e^2/q^2$, we maintain terms with wave vector q close to $q = 0$ that do not cancel with the background and hence give a large contribution to the energy.

As an example of the relevance of this approach for strongly correlated systems we focus on the $t - J$ model, one of the more often used models in the cuprates. The large J/t limit has been studied in detail in two,¹²⁻¹⁴ and more dimensions based on a large d expansion.¹⁵ We study the limiting case of small number of electrons (hole doping close to one). This is not particularly relevant for the cuprates but illustrates the issue of frustrated PS in a strongly correlated system.

A. Maxwell Construction analysis

We start by reviewing the usual MC arguments^{12,15} in the absence of LRC adapted to the 3d case. The antifer-

romagnetic phase at half filling, hereafter the *B* phase, can be model by an incompressible phase with one electron per site. the density is given by $n_B = n_B^0 = 1/a^3$. Our densities refer to real electrons, not to holes. The energy is:

$$f_B = f_B^0 = -3bJn_B^0 \quad (24)$$

where bJ is the magnetic energy per bond. From estimates of the ground state energy in the 3d Heisenberg model¹⁵ one finds $b = 0.550$.

Two different situations are found for the PS. For very large J/t one finds PS between the AF phase and the electron vacuum (AF+V). Reducing J/t one finds PS between the AF phase and a dilute metal of electrons (AF+M). In the first case $f_A = 0$. In the second case the energy of the *A* phase is given by:

$$f_A(n_A) = -6tn_A + \frac{3}{5}3^{2/3}\pi^{4/3}a^2n_A^{5/3}t \quad (25)$$

Here t is the hopping matrix element and we have used the effective mass approximation in the dispersion relation of the low density limit of the $t - J$ model.^{12,15}

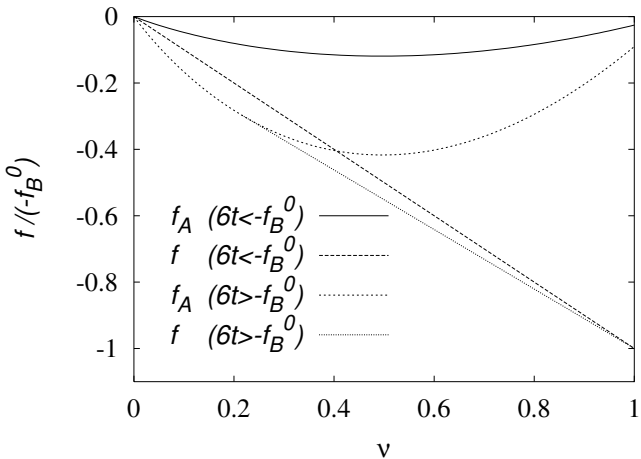


FIG. 11. Free energy normalized to the incompressible phase free energy without LRC and (from top to bottom close to the origin) the metal with $6t = 0.6|f_B^0|$, PS between the AF and vacuum (AF+V), the metal with $6t = 2.1|f_B^0|$, MC phase separation between the AF and the metal (AF+M). ($n_B^0 = a = 1$)

In Fig. 11 we show the free energies in the absence of LRC and different values of $t/(-f_B^0)$. f is given by Eq. (8) with $e_\sigma = e_e = 0$. Since densities are assumed to be low we can neglect the short range interaction between the electrons. We define the number of electrons per unit cell $\nu \equiv n/n_B^0$. In addition we set $a = 1$ and restore it when convenient for clarity.

For very large J/t the AF+V solution is the lowest in energy. Indeed in Fig. 11 the upper curve corresponding to the uniform metallic energy does not intersect

the *AF + V* line, $f = \nu f_B^0$ corresponding to MC between the $\nu = 0$ and $\nu = 1$ points. Decreasing the value of J/t when the chemical potential of the metal fulfills $\mu_A(0)(= -6t) < f_B^0$ i.e. $t > bJ/2$ the metallic free energy intersects the AF+V free energy at some finite density and the lowest energy state is achieved by doing MC between the antiferromagnet and the metal. In this case as shown in Fig. 11, one finds a pure metallic phase at small density and MC phase separation between the AF and the metal for larger density. In Fig. 17 we show the phase diagram deduced from this analysis. The dilute metal can be unstable towards a gas of bound particles.^{12,15} Here we do not consider this effect for simplicity.

In the next two subsections we analyze the effect of the LRC interaction on the AF+V PS and the AF+M PS. Since the electronic free energy has a simple form we solve the equations exactly rather than making a linearization as in Sec. III.

B. Drops of an incompressible phase in vacuum (AF+V)

As shown above this case is realized in the large J/t limit. Now we generalize the above discussion with the inclusion of LRC and surface energy effects. The *A* phase is the electron vacuum (V) ($n_A = 0$ and $f_A = 0$) and the *B* phase is the AF with one electron per site, $n_B = n_B^0 = 1/a^3$ and energy given by Eq. (24). The total free energy is given by Eq. (8) with the above replacements. An expansion of the densities around the MC solution (Sec. III) gives a trivial result since $\lambda = 0$ (notice that $k_m = 0$) and the densities are fixed at the MC values [Eq. (17)]. However this is a peculiar limit. In fact as we will show below the total free energy does not coincide with the MC free energy because of the electrostatic and surface energy contribution. Since the densities are fixed only the radius has to be determined which is given again by Eq. (9).

The surface energy of the AF is given by the energy cost to cut a bond divided the associated surface $\sigma = bJ/a^2$ and the volume fraction is determined by the constraint $x = n/n_B^0 = \nu$. Inserting this in Eq. (9) we obtain:

$$R_d = \left(\frac{15}{8\pi} \frac{bJ}{g(\nu)e^2/a} \right)^{1/3} a \quad (26)$$

The electrostatic energy (and all our formulas) can be renormalized to take into account the dielectric constant of the environment ϵ_0 according to $e^2 \rightarrow e^2/\epsilon_0$. As long as the dielectric constant is sufficiently large the radius is much larger than the lattice spacing and our approximations are valid.

By writing the free energy in dimensionless variables we can define a coupling constant that will determine the transition from the AF+V solution and the AF+M solution in the presence of LRC. It is given by:

$$\alpha = \frac{3}{-f_B^0} \left[\frac{9\pi e^2 \sigma^2 (n_B^0)^2}{5} \right]^{1/3}. \quad (27)$$

Inserting the parameters for AF drops in Eq. (27) we find:

$$\alpha^3 = \frac{9\pi e^2}{5} \frac{a^2}{bJ} \quad (28)$$

i.e. the ratio of a Coulomb energy to a magnetic energy.

Imposing that $R_d > a$ for $\nu = 0$ one finds $\alpha < 3/2$ so we will concentrate on this range of coupling.

From Eqs. (8),(9) we obtain the free energy as a function of density:

$$f(\nu) = \nu[-1 + \alpha g(\nu)^{1/3}](-f_B^0) \quad (29)$$

This is plotted in Fig. 12 for different values of the coupling α . As in the above the results are only rigorously valid for small x ($= \nu$).

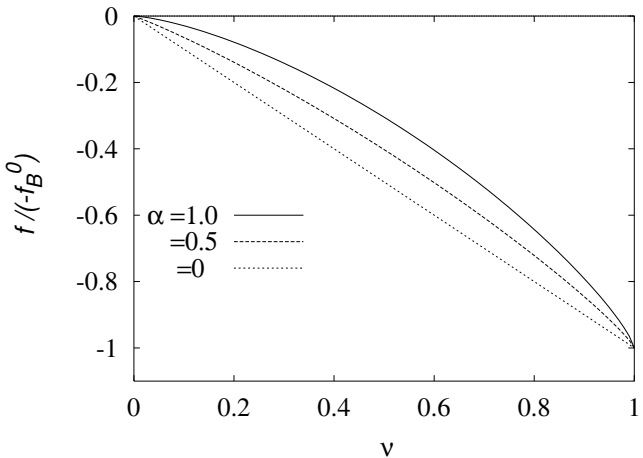


FIG. 12. $f/(-f_B^0)$ for a phase of drops of an incompressible phase in vacuum for $\alpha = 0, 0.5, 1, 2$ (from bottom to top) vs. ν .

The effect of the LRC interaction is to bend upwards the AF+V free energy (see Fig. 12) so that the metallic phase can become stable with a lower value of t with respect with the case with no LRC force (compare with Fig. 11). One can show that for $\alpha > 1$ the AF+V solution is never stable and one has either a uniform metal or an AF+M solution depending on doping. For $\alpha < 1$ the drops can coexist with a metal or not depending on the value of t/J . We will analyze the competition with the AF+M solution in the next section.

C. Drops of an incompressible phase in a metallic host (AF+M)

Reducing J/t at some point the solution of the previous section (AF+V) will not be stable any more. This has

already been shown in the absence of LRC interaction ($\alpha = 0$). We consider now the A phase to be the metal.

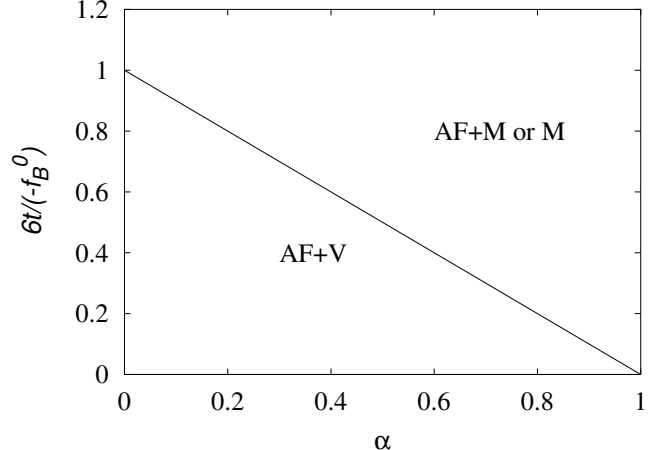


FIG. 13. Locus of stability of the AF drops in vacuum (AF+V) in the $t - \alpha$ plane. Above the line the more stable solution depends on density.

The surface energy will have now density dependent contributions coming from the metal. However, since we are in the low density limit the surface energy will be dominated by the magnetic surface energy described in the previous case and can be taken as constant. The AF+V solution is then not any more stable when $\mu_A(0) = -6t < \mu_{AF+V}(0) = (\alpha - 1)(-f_B^0)$.

In Fig. 13 we show the locus of stability of the AF+V solution in the $t - \alpha$ plane. Above the line the stable solution is either a uniform metal or drops of AF in the metal depending on the density. In Ref. 15 the ratio of J/t below which the AF+V solution is not stable for $\alpha = 0$ is called Y_c . In 2d they found $Y_c(0) = 3.4367$ and $Y_c(0) \rightarrow 4$ for $d \rightarrow \infty$.¹⁵ Using their estimate of the 3d AF energy we have $Y_c(0) = 3.637$. Fig. 13 shows that Y_c (proportional to the critical value of $-f_B^0/6t$) increases with α . Remarkably in the presence of LRC forces a smaller t is enough to stabilize metallic phase regions. In other words we can have a situation in which without LRC forces all the electrons are in a self bounded AF state and as the LRC forces are switched-on some electrons “evaporate” to form a dilute gas around the AF drops.

To solve for the AF+M drop solution the free energy now has to be minimized with respect to the radius and the density of the metal subject to the constraint $n = xn_B^0 + (1 - x)n_A$. We are implicitly assuming that the density is not low enough to form a Wigner crystal of electrons. One can check that for reasonable parameters and increasing α the radius of the drop becomes of the order of the lattice constant much before an electronic Wigner crystal can form.

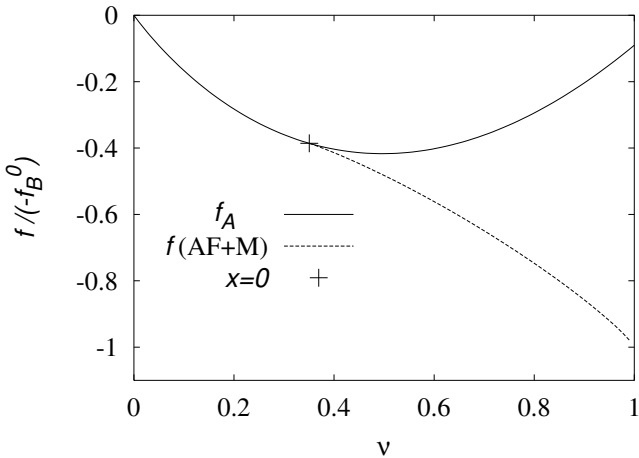


FIG. 14. Free energy normalized to the incompressible phase free energy with parameters $\alpha = 0.5$ and $6t = 2.1|f_B^0|$. We show the metallic free energy, the AF+V free energy and the AF+M free energy. The cross indicates the value with $x = 0$ of the AF+M drop solution.

Above the boundary line on Fig. 13 one finds either a uniform metal or AF+M depending on density. This can be seen in Fig. 14 where we plot the free energies for $6t = 2.1|f_B^0|$ and $\alpha = 0.5$. Above a certain density $n_{bif} = \nu_{bif}/a^3$ we have coexistence of AF drops in the metallic host. The behavior close to n_{bif} is very similar to the behavior shown in Sec. III.

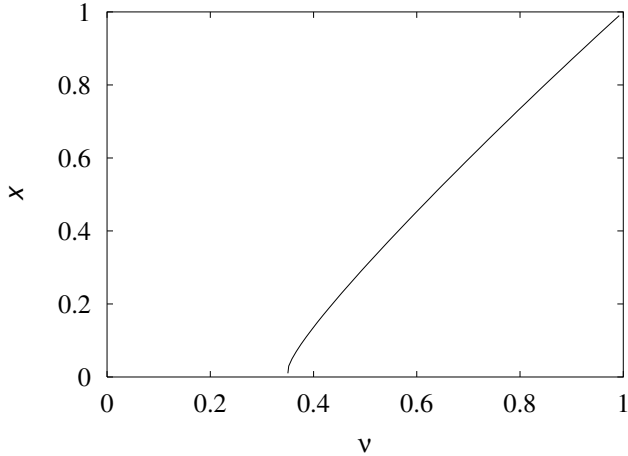


FIG. 15. Volume fraction vs. ν for AF drops in a metallic host and parameters as in Fig. 14.

Here also there is a bifurcation of the solution and increasing the density, the AF drops appear with a nonzero value of the volume fraction. However with the present parameters the initial volume fraction is very small (See Fig. 15).

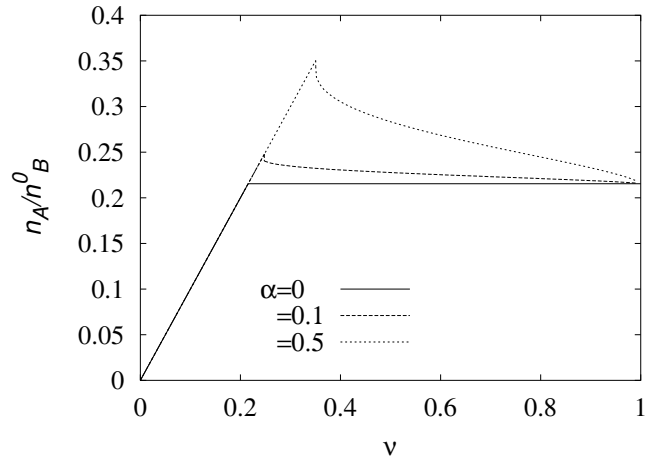


FIG. 16. Density in the metallic host vs. total density ν for $6t = 2.1|f_B^0|$ and different values of α .

As the B density grows the n_A density decreases due to the effect discussed in Sec. III. The only difference is that the B density is kept constant at n_B^0 due to the incompressibility. In Fig. 16 we show this behavior. In real systems this effect can be detected through physical properties which depend on the local densities as is discussed below for the manganites.

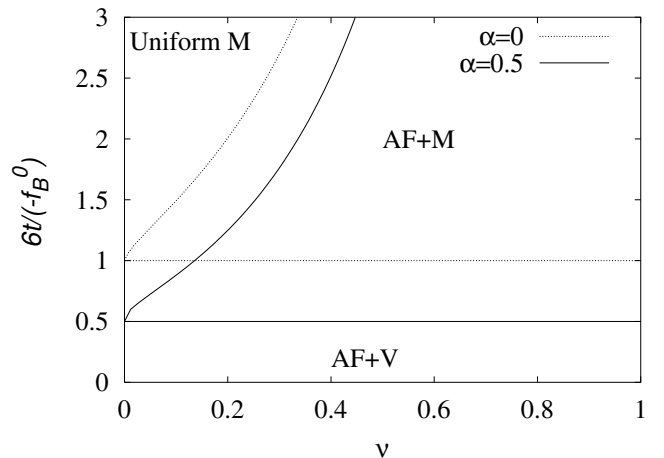


FIG. 17. Phase diagram for the large J/t limit of the 3D $t - J$ model without LRC ($\alpha = 0$) and with a small LRC ($\alpha = 0.5$). The high density part has to be taken with care since the density of electrons can be large in the metal so that short range interactions within the metallic phase cannot be neglected any more, and also drops of AF loose sense.

In Fig. 17 we show the phase diagram in the absence of LRC force ($\alpha = 0$) and for $\alpha = 0.5$. We see that a portion of the phase diagram in which a uniform solution is unstable towards PS without LRC, for $\alpha > 0$ becomes

stable and the AF+M solution extends its region with respect to the AF+V solution due to the “evaporation” effect.

VI. APPLICATION TO THE MANGANITES

As a further application we consider the magnetoresistive manganites³ like $\text{La}_{1-y}\text{Ca}_y\text{MnO}_3$. In the last years strong experimental evidence has accumulated indicating that inhomogeneous phase separation occurs in these materials in certain regions of parameter space^{16–19,11,20}.

At $y = 0$ all Mn have formal valence 3+. Each ion has three electrons in t_{2g} orbitals and one electron in an e_g orbital. The four electrons spins are all parallel due to the strong Hund’s rule coupling forming an $S = 2$ spin. The spins of different Mn³⁺ ions form an antiferromagnetic (AF) phase due to the superexchange interaction and the system is an insulator. As the e_g band is doped, mobile holes tend to align the $S = 3/2$ core (t_{2g}) spins in different ions because this maximizes the transfer integral and minimize the holes kinetic energy leading to a ferromagnetic state. This is the so called double exchange (DE) mechanism^{21–23}.

Experimentally one finds indeed the ferromagnetic state but close to $y = 0.5$ a new charge ordered (CO) insulating phase with a chessboard structure of Mn³⁺ and Mn⁴⁺ is stabilized. The CO phase is not predicted by the conventional DE but does appear in more recent theories incorporating Mn-Mn Coulomb repulsion²⁴ or orbital degrees of freedom²⁵.

Close to $y = 0$ and $y = 0.5$ the metallic ferromagnetic (FM) phase competes with the corresponding insulating phase. The drop state due to the competition between the $y = 0$ AF phase and the metallic phase taking into account the LRC interaction has been studied theoretically by Nagaev and collaborators^{4,5}. Evidence for such a phase has recently been found in neutron scattering experiments¹⁹.

Here we will analyze the competition of the CO phase with the FM phase close to $y = 0.5$ and show that a phase separated state can explain the puzzling maximum of the Curie temperature $T_c(y)$ at $y \sim 0.35$ ^{26,27}. On the contrary, conventional DE would predict that the Curie temperature is maximum at half doping ($y = 0.5$) because for this filling the kinetic energy of the holes is maximized.

We will consider a mixed state in which the A phase is the ferromagnetic metal (FM) and the B phase is the charge order state at $y = 0.5$ which corresponds to inverse specific volume $n_B^0 = 0.5/a^3$. In the following the densities refer to holes (i.e. the concentration of Mn⁴⁺ ions).

In the FM phase the core spins of the Mn ions are fully polarized and the mobile holes have the maximum bandwidth W . In order to model the FM in a simple

fashion we follow Varma²⁸ and take a flat density of states with bandwidth W . The FM free energy at $T = 0$ is then given by the cohesive energy of the holes in the fully polarized state:

$$f_A(n_A) = \frac{Wa^3}{2}(n_A - n_B^0)^2. \quad (30)$$

We have chosen to measure the single particle energies from the center of the band and we have dropped a constant which can be absorbed in the free energy constant of the B phase f_B^0 . At finite temperatures one has to consider the entropy contribution to the free energy. However for a given temperature one can expand the full A free energy around the n_B^0 density and an expression like Eq. (30) is still valid with an effective temperature dependent W .

The CO state can be modelled as a doped incompressible phase around the inverse specific volume n_B^0 . The free energy at $T = 0$ can be put as:

$$f_B(n_B) = \frac{E_G}{2}|n_B - n_B^0| + e_0(n_B - n_B^0) + f_B^0. \quad (31)$$

f_B^0 measures the difference in free energy per hole between the CO state and the FM state at $y = 0.5$ ($n = n_B^0$) and e_0 controls the difference in chemical potentials of the two phases. E_G is the gap in the charge order state. i.e. the difference between the energies to create defects with one added hole and one removed hole without destroying the CO state. (It should be of the order of the activation energy in the transport properties of a pure CO state). The dip in the free energy at $n = n_B^0$ will become rounded with temperature. For simplicity we will neglect this effect. For temperatures much smaller than the gap this is a good approximation. Even if the temperature gets comparable to the gap a small rounding of the CO free energy close to $n_B = n_B^0$ will not affect significantly the results close to the density at which drops first appear (n_{bif}).

The chemical potential of the CO state at $T = 0$ is given by:

$$\mu^+ = e_0 + E_g/2 \quad n_B > n_B^0 \quad (32)$$

$$\mu^- = e_0 - E_g/2 \quad n_B < n_B^0. \quad (33)$$

By construction the discontinuity at n_B^0 is equal to the gap as it should be. μ^- is the energy to create a Mn³⁺ defect in the CO state. i.e. it is the energy to remove a hole in the CO state. This single particle energy is measured from the same reference energy as the one used for the A phase in Eq. (30). This fixes the value of e_0 .

In Fig. 18 we have plotted f_A , f_B as a function of y . We constructed the free energies for the uniform phases phenomenologically, by relying on the metallic and insulating character of each phase and on the fact that due to the different magnetic symmetry they cannot be joint with continuity but a level crossing should occur as a

function of y . It is interesting to note that a recent microscopic model gives practically the same energy scheme as a function of doping²⁵.

In Fig. 18 we report also the MC and the free energy for the drop solution for $\alpha = 3$ and $W' \equiv Wn_B^0/(-f_0^B) = 15$ (thick line). The coupling constant α is defined in Eq. (27). W' measures the effective bandwidth in units of $(-f_0^B)$.

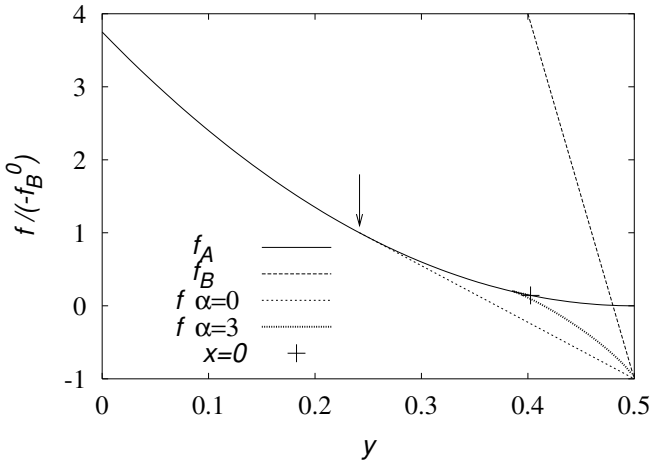


FIG. 18. Free energy normalized to the incompressible phase free energy at $y = 0.5$ with a bandwidth $W = 15|f_B^0|/n_B^0$. We show the FM free energy (f_A), the CO free energy with a large negative value of μ^- , the FM+CO free energy for $\alpha = 0$ (MC), and for $\alpha = 3$. The cross indicates the value with $x = 0$ of the FM+CO drop solution. The arrow indicates the same for MC (y_0).

For the sake of simplicity we assume that the slope of f_B for $n_B < n_B^0$ (i.e. μ^-) is so large that f_B never crosses the drop solution. Under these simplifying condition one of the phases involved in phase separation is always the defect free CO state at $y = 0.5$. In this situation E_g and e_0 do not enter into the problem and a precise description of $f_B(n_B)$ is not needed. For example we have neglected the kinetic energy of the defects which will give some curvature to $f_B(n_B)$ but will not change the present picture.

Alternatively to α we could use the coupling constant λ defined in Sec. III since the FM free energy is parabolic ($k_A^{-1} = k_m^{-1} = Wa^3$) and the CO free energy can be consider as the $k_B \rightarrow 0$ limit of a parabola. The two coupling constants are related by

$$\lambda = \frac{2^{2/3}}{3} \frac{\alpha}{(W')^{1/3}}. \quad (34)$$

Specifically $\lambda = 0.64$ for $\alpha = 3$ and $W' = 15$. Notice however that here (as in the previous section) we can introduce two dimensionless parameters. One is α (or alternatively λ) and the other is W' . The latter plays the

same role as t/J in the previous section. In particular it fixes the MC densities as follows. In the absence of LRC interaction ($\alpha = 0$) and for $W' < 4$ the f_A parabola is too flat and PS between the FM and the CO state is not possible. One gets PS between the CO state and vacuum (this is similar to the AF+V PS considered in Sec. V B). For $W' > 4$ Maxwell construction gives PS between FM and CO with the critical doping given by:

$$y_0 = \frac{1}{2} - \frac{1}{\sqrt{W'}} \quad (35)$$

In Fig. 18 the value of y_0 is indicated by an arrow.

In the presence of LRC interaction the range of coexistence contracts with respect to the Maxwell construction case. The transition from the FM to the drop solution is quite abrupt at $y_{bif} = 0.38$ (for $\alpha = 3$) with a substantial jump of the volume fraction from zero to a finite value $x_{bif} = 0.17$. (See Fig. 19).

In Fig. 20 we show the local density inside the metallic region. For $y < y_{bif}$ the stable phase is uniform FM and the total density coincides with the nominal density $n = y/a^3$. For $y > y_{bif}$ the drop solution is stable and the density in the metallic region decreases with increasing nominal density. As discussed in Sec. III, in deriving this effect it is important that the density dependence of the surface energy can be neglected. The strongest dependence of the surface energy is expected to arise from the kinetic energy of the metal. However, this dependence is important close to $y \sim 1$ and $y \sim 0$ and can be safely neglected close to $y \sim 0.5$.

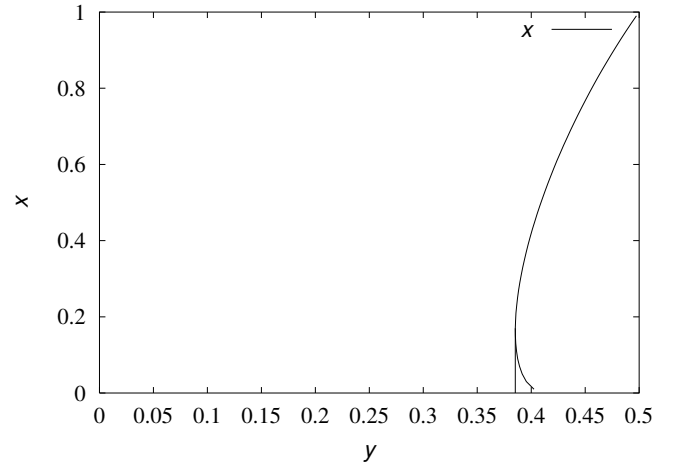


FIG. 19. Volume fraction vs. y for CO drops in a FM host and parameters as in Fig. 18. The lower branch close to $y \sim 0.4$ is unphysical.

The decrease of local density with increase of global density can explain the non-monotonous dependence of Curie temperature T_c on y . Since the ferromagnetic interaction between the core Mn spins is mediated by

the conduction electrons through the double exchange mechanism one expects the Curie temperature to be a monotonous increasing function of the local metallic density $n_A (< n_B^0)$ of the FM phase. We associate the region in which the Curie temperature increases with doping, i.e. the “normal” region (roughly $0.1 < y < 0.33$ for $\text{La}_{1-y}\text{Ca}_y\text{MnO}_3$), with a uniform FM phase and the “anomalous” regions in which the Curie temperature decreases with doping with a drop state. In the latter state n_A decreases with doping and this gives the anomalous behavior of T_c as a function of doping.

To be more specific we assume the following simple form for the dependence of the Curie temperature on the local FM density:

$$\frac{t_c(a^3 n_A) - t_c(0)}{t_c(0.5) - t_c(0)} = 4(1 - a^3 n_A) * a^3 n_A \quad (36)$$

We are using uncapitalized t for the local Curie temperature of the FM phase to distinguish it from the true Curie temperature of the system which is a function of the overall doping $T_c(y)$. A similar form as Eq. (36) with $t_c(0) = 0$ was derived by Varma for a uniform FM phase.²⁸ More sophisticated treatments also give a form roughly parabolic with $t_c(0) > 0$.²⁹

For a uniform FM phase $y = n_A a^3$, $T_c(y) = t_c(y)$. This fits correctly the experimental data in the normal region. We can use this fit to fix the parameters in Eq. (36). For $\text{La}_{1-y}\text{Ca}_y\text{MnO}_3$ one obtains $t_c(0) \sim 80\text{K}$ and $t_c(0.5) \sim 300\text{K}$. Close to $y = 0.5$ [$y = 0$] we have the anomalous behavior and the measured T_c differs considerably from $t_c(0.5)$ [$t_c(0)$], the Curie temperature of an hypothetically uniform phase. For example, experimentally $T_c(0.5) \sim 225\text{K}$.

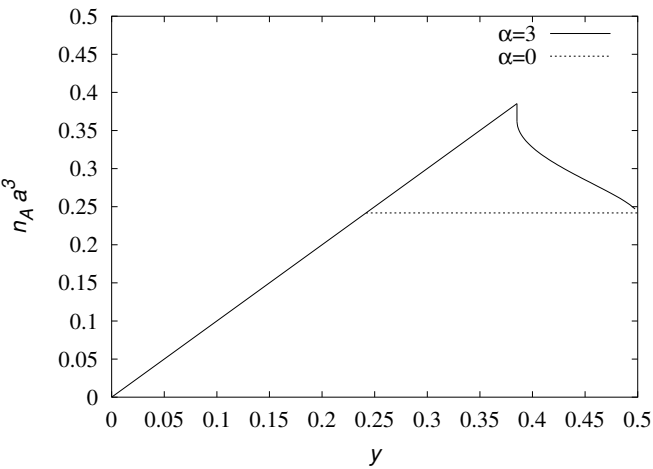


FIG. 20. Density in the metallic host vs. doping y for parameters as in Fig. 18.

From the known $n_A(y)$ (Fig. 20) and Eq. (36) we compute $T_c(y) \equiv t_c[a^3 n_A(y)]$. This curve (which is quite similar to the experimental one) is shown in Fig. 21. Indeed

we see that the drop solution combined with the uniform solution for $y < y_{bif}$ gives a non-monotonous behavior of $T_c(y)$. In evaluating the theoretical curve to be compared with the experimental data we fix the values of α and W' in the following way. We associate the experimental maximum in T_c with the bifurcation point, i.e. the doping at which the uniform solution switches to the drop solution. This gives us an experimental value of the bifurcation doping $y_{bif} \sim 0.38$. From the experimental data we also obtain the depression of the Curie temperature $[T_c(0.5) - t_c(0)]/[t_c(0.5) - t_c(0)] \sim 0.66$. With these two dimensionless numbers we obtain the dimensionless parameters of our theory and find $\alpha = 3$ and $W' = 15$ i.e. the values that we have been using in the present section. A rough microscopic estimate of these parameters is given in Appendix B to show that indeed the above values are reasonable for the manganites.

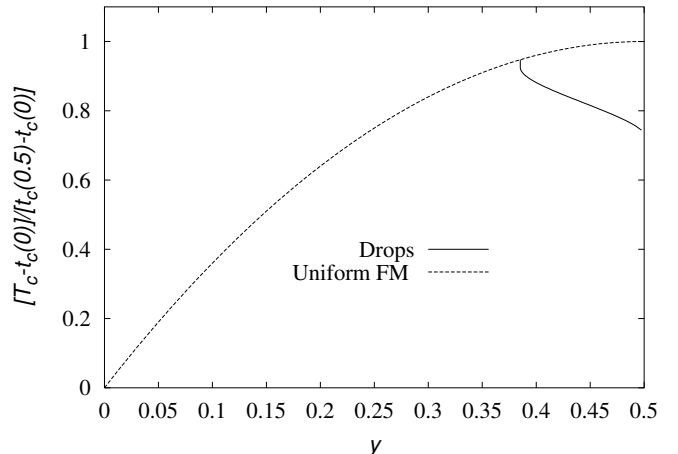


FIG. 21. T_c of the FM host minus $t_c(0)$ normalized to $t_c(0.5) - t_c(0)$ as a function of doping y . Parameters are as in Fig. 18. We show the T_c in the uniform solution and in the drop solution.

VII. CONCLUSIONS

In this work we have generalized the Maxwell construction to a situation that appears often in strongly correlated electronic systems, i.e. phase separation frustrated by the long range Coulomb interaction. As it is intuitively expected, the LRC interaction tends to stabilize the non-separated uniform phases in the presence of a rigid background. This has been illustrated in the general analysis of two generic phases described by parabolic free energies and in the case of the $t - J$ model. We showed that the region of phase separation contracts as the LRC and surface energy effects are switched on and disappears above a critical value of a dimensionless parameter λ . This parameter, which plays the role of an effective coupling, characterizes the competition between the energy

cost, due to the surface energy and LRC effects, and the energy gain in the MC. The balance between these energies determine if the phase separated state exists or not.

In the case of strong Coulomb interaction and large surface energy (i.e. large λ) a transition between two uniform phases can occur. We have shown that in this case the compressibility is singular and a lattice instability will take place if the ionic background is not fully rigid. The system (both electrons and ions) separates in two neutral phases with different specific volumes.

When λ is not so large a mixed state arises. We have modeled this situation by considering a Wigner crystal of drops of one phase hosted by the other. We believe that our general conclusions are not sensitive to the geometry of the mixed state as long as the two length scales R_c and R_d are present and both are much larger than the interparticle distance. The former length (cell size) characterizes a periodic structure and the latter (bubble size) how this periodic structure is divided to host the two phases. An indication that the geometry is not very important comes from the fact that the plots of the physical quantities in Sec. III for $k_A = k_B$ are quite symmetric to an exchange of the two phases, each one having a different shape. This means that the behavior of the drops is not much different from the behavior of their counterpart, the interstitial regions.

When do we expect such a mesoscopic phase separation to prevail against microscopic phase separation (like stripes)? From the drop volume $R_d^3 \sim \sigma\epsilon_0/(e^2\delta^2)$ [where the effective dielectric constant has been introduced with respect to Eq. (9)] we see that large drops can be expected when the surface energy is large or the Coulomb energy is small. A small Coulomb energy can arise due to strong screening effects or because the two competing phases have very similar densities making δ small. This can be achieved in the manganites where a variety of different ground states with close densities have similar energies. By contrast, in the case of the Wigner crystal of electrons (where the energy gain from MC has an electrostatic origin as the energy cost) the Coulomb strength and the surface energy balance in such a way that large drops are not possible.

Notice that the condition for the existence of the mixed phase-separated state ($\lambda < \lambda_c$) and the condition for large drops are different since in the former case the surface energy and the electronic charge contribute in the same direction whereas in the later case they play opposite roles.

In the mixed state novel non-linear effects appear which are not present in the unfrustrated MC. The volume fraction and the drop radius of the minority phase do not start from zero but from a finite value and the transition to the drops state is abrupt. In principle also at the transition point to the drop state a lattice instability can arise for the same reasons discussed for large λ , although the instability is now much weaker. We mention that these lattice instabilities, which also involve volume

variations, are reminiscent of the macroscopic phase separation observed in some manganites.¹¹

Apart from the stabilization of the uniform phases the LRC interaction can also favor one mixed state over another. This was illustrated in the case of the $t - J$ model where the LRC interaction can transform a selfbound state of electrons in vacuum into a selfbound state of electrons in equilibrium with its vapor, a phenomenon which we referred to as “evaporation”.

A further non-linear effect in the drop state is that the local densities of each phase have an anomalous behavior decreasing as the global density increases. This can affect properties of the system which are sensitive to the local density, as we have illustrated for the Curie temperature in the manganites. We emphasize that also local probes like NMR, core spectroscopy etc. should be sensitive to this effect and may be used to detect Coulomb frustrated phase separation in real systems.

APPENDIX A: CORRECTION DUE TO DISCREETNESS OF THE CHARGE

In order to compute the electrostatic energy in the drop solution [Eq. (6)] we assume that the charge within one drop is spread uniformly. Variations of density can arise because of Volta effects as discussed in Sec. II and because of intrinsic charge inhomogeneities as in a charge density wave. Here we discuss the latter effect.

Let us now consider the opposite limit and assume that both phases A and B are two Wigner crystals of electrons as a prototypical case in which the charge is intrinsically non-uniform. What is the correction to the Eq. (6)?

In the host phase we neglected the interaction between the neutral A Wigner crystal of electrons and a background of charge density $(n - n_A)e$ (see Fig. 1). The fluctuation of the charge inside the crystalline Wigner-Seitz cell can make this interaction nonzero. Also for the phase forming the drop we have to consider the interaction between the neutral B Wigner crystal and a background of charge density $(n - n_B)e$.

The electrostatic contribution per drop is:

$$\epsilon_{A-b} = -\frac{3eq_A}{10r_A} N_A$$

with

$$q_A = \frac{4\pi}{3} r_A^3 (n - n_A) e$$

and a similar expressions for the B phase. Here $\frac{4\pi}{3} r_A^3 = 1/n_A$ and N_A is the number of electrons of A phase in a drop:

$$N_A = n_A v_d \left(\frac{1}{x} - 1 \right)$$

$$N_B = n_B v_d$$

The total contribution per unit volume to the electrostatic energy is:

$$\Delta e_e = \frac{2\pi e^2}{5} [(n_B - n)n_B r_B^2 x + (n_A - n)n_A r_A^2 (1 - x)] \quad (\text{A1})$$

Clearly [c.f. Eq. (6)] the correction $\Delta e_e/e_e$ is of order $r_{A,B}^2/R_d^2$ so it is negligible unless the volume of the drop is of the order of the volume per particle in which case the whole computation has no sense.

APPENDIX B: MICROSCOPIC ESTIMATE OF PARAMETERS IN THE MANGANITES

In Sec. VI we find that the parameters $\lambda = 0.64$ and $W' = 15$ give a curve $T_c(y)$ similar to the experimental one. To decide if these parameters are reasonable one needs a microscopic computation.

To evaluate W' which appears in Eq. (35) we refer to a recent zero temperature microscopic computation which takes into account double exchange and orbital ordering.²⁵ Their Fig. 2 showing the free energy (without LRC) is quite similar to our $\alpha = 0$ curves in Fig. 18. From there we take $y_0 \sim 0.24$ which determines $W' \sim 15$ [Eq. (35)] in agreement with the value we used to fit T_c . λ is more difficult to obtain because it requires a microscopic computation of surface energies and screening effects. We parameterize the surface energy by a dimensionless quantity γ defined by $\sigma \equiv \gamma W/a^2$. Putting $\delta_0 = (0.5 - y_0)/a^3$ and $k_A^{-1} = k_m^{-1} = Wa^3$ in Eq. (13) we get:

$$\lambda = 2 \left(\frac{9\pi}{5} \right)^{1/3} \frac{\gamma^{2/3}}{(0.5 - y_0)^{4/3}} \left(\frac{e^2}{\epsilon_0 a W} \right)^{1/3} \quad (\text{B1})$$

where the dielectric constant has been introduced in Eq. (13). For the bandwidth we can take an estimate based on Mattheiss's local density approximation (See Ref. 28) $W = 2.5\text{eV}$. For a cubic array of Mn with a Mn-Mn distance of 4Å we get $\frac{e^2}{a} = 3.4\text{eV}$ for the bare Coulomb strength. Inserting the numerical values in the above equation we have

$$\lambda \sim 21 \left(\frac{\gamma^2}{\epsilon_0} \right)^{1/3}$$

One obtains $\lambda \sim 0.64$, the value we have used in Sec. VI, by taking $\epsilon_0 \sim 100$ and $\gamma \sim 0.05$. These are reasonable parameters considering that ϵ_0 should be understood as a static dielectric constant taking into account conventional dielectric screening plus non-linear Thomas Fermi screening effects (Sec. II) etc. and γW should be a small fraction of the bandwidth.

We mention that since a real background is never perfectly rigid, a volume relaxation will also occur inside the drop phase. In general the positive background will

contract in the electron rich phase and expand in the electron poor phase to reduce the mismatch between the ionic positive density and the electronic density. This is in agreement with the situation in $\text{Pr}_{0.7}\text{Ca}_{0.3}\text{MnO}_3$ where the electron poor CO phase has a larger volume than the electron rich FM phase¹⁸. Clearly this effect will contribute to produce larger values of the effective dielectric constant ϵ_0 .

The drop radius reads:

$$R_d = \frac{3}{\lambda} \frac{\gamma a}{[(\delta a^3)^2 (0.5 - y_0)^4 g(x)]^{1/3}} \quad (\text{B2})$$

Using the above parameters we can estimate the radius at the onset ($x_{\text{bif}} = 0.17$) to be of the order of

$$R_d \sim 10a$$

Correspondingly the cell radius is $R_c = R_d/x^{1/3} \sim 18a$. We see that these scales are much larger than the lattice constant and our approximations apply.

* On leave of absence from Consejo Nacional de Investigaciones Científicas y Técnicas, Centro Atómico Bariloche, 8400 S. C. de Bariloche, Argentina.

¹ in *Phase separation in cuprate superconductors*, edited by K. A. Muller and G. Benedek (World Scientific, Singapore, 1992).

² in *Phase separation in cuprate superconductors*, edited by E. Sigmund and K. A. Muller (Springer-Verlag, Berlin, 1993).

³ A. Moreo, S. Yunoki, and E. Dagotto, *Science* **283**, 2034 (1999).

⁴ E. Nagaev, *Physics of magnetic semiconductors* (MIR, Moscow, 1983).

⁵ E. Nagaev, A. I. Podel'shchikov, and V. E. Zil'bawarg, *J. Phys.: Condens. Matter* **10**, 9823 (1998).

⁶ U. Löw, V. J. Emery, K. Fabricius, and S. A. Kivelson, *Phys. Rev. Lett.* **72**, 1918 (1994).

⁷ C. Castellani, C. Di Castro, and M. Grilli, *Phys. Rev. Lett.* **75**, 4650 (1995).

⁸ M. Y. Kagan, K. I. Kugel, and D. I. Khomskii, cond-mat/0001245 (unpublished).

⁹ E. Wigner, *Phys. Rev.* **46**, 1002 (1934).

¹⁰ G. D. Mahan, *Many Particle Physics* (Plenum, New York, 1990).

¹¹ M. Uehara, S. Mori, C. Chen, and S.-W. Cheong, *Nature* (London) **399**, 560 (1999).

¹² V. J. Emery, S. A. Kivelson, and H. Q. Lin, *Phys. Rev. Lett.* **64**, 475 (1990).

¹³ M. Calandra, F. Becca, and S. Sorella, *Phys. Rev. Lett.* **81**, 5185 (1998).

¹⁴ S. R. White, *Phys. Rev. B* **61**, 6320 (2000).

¹⁵ E. Carlson, S. A. Kivelson, Z. Nussinov, and V. Emery, *Phys. Rev. B* **57**, 14704 (1998).

¹⁶ J. W. Lynn *et al.*, Phys. Rev. Lett. **76**, 4046 (1996).

¹⁷ J. De Teresa *et al.*, Nature (London) **386**, 256 (1997).

¹⁸ D. E. Cox *et al.*, Phys. Rev. B **57**, 3305 (1998).

¹⁹ M. Hennion *et al.*, Phys. Rev. Lett. **81**, 1957 (1998).

²⁰ G. Papavassiliou *et al.*, Phys. Rev. Lett. **84**, 761 (2000).

²¹ C. Zener, Phys. Rev. **82**, 403 (1951).

²² P. W. Anderson and H. Hasegawa, Phys. Rev. **100**, 675 (1955).

²³ P. G. de Gennes, Phys. Rev. **118**, 141 (1960).

²⁴ M. Y. Kagan, D. I. Khomskii, and M. V. Mostovoy, Eur. Phys. J. B **12**, 217 (1999).

²⁵ J. van der Brink, G. Khaliullin, and D. Khomskii, Phys. Rev. Lett. **83**, 5118 (1999).

²⁶ P. Schiffer, A. P. Ramirez, W. Bao, and S.-W. Cheong, Phys. Rev. Lett. **75**, 336 (1995).

²⁷ K. H. Kim, M. Uehara, and S.-W. Cheong, cond-mat/0004467 (unpublished).

²⁸ C. M. Varma, Phys. Rev. B **54**, 7328 (1996).

²⁹ S. Okamoto, S. Ishihara, and S. Maekawa, Phys. Rev. B **61**, 451 (2000).